Anesthesiology 2003; 99:638–45

Model Predictions of Gas Embolism Growth and Reabsorption during Xenon Anesthesia

Naomi Sta Maria, B.S., David M. Eckmann, Ph.D., M.D.†*

Background: **It is not readily obvious whether an intravascular bubble will grow or shrink in a particular tissue bed. This depends on the constituent gases initially present in the bubble, the surrounding tissue, and the delivered gas admixture. The authors used a computational model based on the physics of gas exchange to predict cerebrovascular embolism behavior during xenon anesthesia.**

Methods: **The authors estimated values of gas transport parameters missing from the literature. The computational model was used with those parameters to predict bubble size over time for a range of temperatures (18°–39°C) used during extracorporeal circulation.**

Results: **Bubble size over time is highly nonlinearly dependent on multiple factors, including diffusivity, solubility, gas partial pressures, magnitude of concentration gradients, vessel diameter, and temperature. Xenon- and oxygen-containing bubbles continue to grow during xenon delivery. Bubble volume doubles from 50 to 100 nl in approximately 3–68 min, depending on initial gas composition and bubble shape. Bubble growth and reabsorption are relatively insensitive to temperature in the physiologic and surgical range.**

Conclusions: **Xenon anesthesia results in gas exchange conditions that favor bubble growth, which may worsen neurologic injury from gas embolism. The concentration gradients can be manipulated by discontinuation of xenon delivery to promote reabsorption of xenon-containing bubbles. Estimated growth and reabsorption rates at normothermia can be applied to temperature extremes of cardiopulmonary bypass.**

FOR more than five decades, the noble gas xenon (Xe) has been known to possess anesthetic properties.[1] Within the past 10 yr, Xe has been increasingly investigated as a potential clinical inhaled anesthetic, primarily due to the homodynamic stability profile associated with its use.[2] Xe does not depress myocardial contractility, alter mesenteric vascular resistance, or potentiate arrhythmias in the presence of epinephrine.[3] Xe is nearly inert chemically, and it is not metabolized. The minimum alveolar concentration (MAC) of Xe is 0.71,[4] and Xe anesthesia is characterized by rapid induction, fast emergence, adequate analgesia and amnesia, and minimal disturbance of pulmonary function. Xe seems to confer some advantage over other inhaled anesthetic agents in the care of patients in whom careful maintenance of cardiovascular stability is required. This includes the treatment of patients undergoing cardiopulmonary bypass and patients with obstruction of a hollow viscus.

The transport properties of Xe in tissue and blood are characteristically similar to those of nitrous oxide. There is a propensity, then, for Xe to be transported out of the dissolved state and to diffuse into gas-filled spaces. This poses a potential risk of growth of trapped gas in the case of bowel obstruction or the enlargement of gas embolism bubbles. One important aspect of assessing the safety of Xe anesthesia in the context of cardiopulmonary bypass is the potential contribution of the inert species to growth of cerebrovascular gas emboli. Some recent experiments of bubbles in aqueous solution have shown that Xe promotes bubble growth.[5] However, it is not readily obvious whether an intravascular (or intraluminal) bubble will grow or shrink *in vivo* in a particular tissue bed. This will depend on multiple factors including the constituent gases initially present in the bubble, their concentrations in surrounding tissue, the ventilation gas, the temperature dependence of gas solubility and diffusivity, and elements of local blood flow.

We hypothesized that bubbles would grow in the presence of Xe in the ventilation admixture and, hence, in tissue. We also hypothesized that the competing effects of temperature on gas solubility and diffusivity would render bubble growth relatively insensitive to temperature in the range of temperatures used in extracorporeal circulation. To assess the effects of Xe on bubble size, we used a mathematical model based on our previous treatments of the physics of gas exchange[6–9] to predict the time-dependent volume of gas embolism bubbles in cerebral and other tissues. We considered combinations of Xe and oxygen in both the initial gas composition of the bubble and the surrounding tissues. We incorporated temperature effects in the range of temperatures commonly encountered during cooling and rewarming phases of cardiopulmonary bypass.

Methods

The theoretical model we developed to calculate bubble volume over time has been described in detail previously[6,8] but is reviewed briefly. The *in vivo* bubble shape is modeled as a cylinder of initial length L_o with hemispherical end caps of initial radius R_o. Based on *in vivo* findings,[6,7,9] we stipulate that as gas moves in or out of the bubble, the cylindrical portion of the embolism

* Research Assistant, Department of Biomedical Engineering, † Assistant Professor, Department of Anesthesia and Institute for Medicine and Engineering.

Received from the Department of Biomedical Engineering, the Department of Anesthesia, and the Institute for Medicine and Engineering, University of Pennsylvania, Philadelphia, Pennsylvania. Submitted for publication December 30, 2002. Accepted for publication April 30, 2003. Supported by a grant from AGA-Linde Healthcare, Lidingo, Sweden, and by grant Nos. HL-60230 and HL-67986 from the National Heart, Lung and Blood Institute, Bethesda, Maryland. Presented in part at the Hauptstadtkongress für Anästhesiologie und Intensivtherapie 2002 Meeting, Berlin, Germany, May 2, 2002.

Address reprint requests to Dr. Eckmann: Department of Anesthesia, University of Pennsylvania, 3400 Spruce Street, Philadelphia, Pennsylvania 19104. Address electronic mail to: EckmannDM@uphs.upenn.edu.

elongates or shrinks, respectively, while the hemispherical end cap radius remains fixed. For bubble shrinkage, when the cylindrical portion completely disappears, the remaining hemispherical end caps coalesce to form a sphere. Spherical geometry is maintained for the remainder of bubble absorption. Bubble absorption is solved independently for two separate temporal phases, the cylindrical phase and the spherical phase. In each case, the law of Fick is applied to the specific bubble geometry. Bubble absorption time depends on the initial aspect ratio of the bubble itself, or L_o/R_o. In the case of bubble elongation, the cylindrical portion gains length, and the hemispherical end cap radius remains constant.

During bubble growth or shrinkage, the mathematical expression for the bubble's internal pressure is based on several assumptions. We assume that rapid equilibrium of carbon dioxide and water vapor occurs between the inside of the bubble and the tissue, with maintenance of constant tissue partial pressure of these gases. Capillary perfusion from surrounding vessels is assumed to convect gas to or from tissue near the bubble, with diffusion accounting for gas transport across the bubble interface. The hydrostatic head of blood pressure is ignored because it is assumed to be small compared to the external barometric pressure. Any elastic force exerted by the vessel wall on the bubble is also neglected because changes in vessel diameter would only cause the bubble to lengthen or shorten, without an increase or decrease in internal pressure. Following the law of LaPlace, the pressure inside the bubble is only balanced by a surface tension term proportional to the inverse of the bubble radius and the difference between the external pressure acting on the bubble and the partial pressures of Xe, oxygen, carbon dioxide, and water vapor in the tissue. We consider cases in which complete nitrogen elimination has occurred, representative of a non–air-containing ventilation admixture for cardiac surgery. The internal bubble pressure, therefore, remains fixed during shrinkage or growth of the cylindrical portion because of a constant value of R_o. During absorption of spherical bubbles, the radius decreases. Consequently, the internal pressure increases. The exchangeable gases oxygen and Xe follow their concentration gradients, diffusing into the bubble if the tissue concentration exceeds the bubble concentration, and diffusing out of the bubble if the tissue concentration is lower. Gases moving into and out of the bubble can slow absorption or even promote bubble growth. With this model, we can numerically determine the time-dependent size of an intravascular bubble over a range of geometries for a given initial volume, temperature, and initial gas content in the bubble and the delivered gas admixture. Knowing local tissue characteristics allows further application to specific areas such as the brain.

The governing transport equation for the model is derived from the two initial equations, the diffusion equation, balancing the bubble volume with the flux of gas across the bubble surface, and the law of LaPlace, balancing the pressure difference across the bubble surface with the surface tension and the interfacial curvature (see Branger and Eckmann[6] for detail). In this analysis, an accounting for each of the gas species being transported must be made as was done by Branger *et al.*[8] The resultant nonlinear time-dependent governing ordinary differential equation (see Branger and Eckmann[6] for explicit derivation) depends on multiple parameters, including the temperature-dependent brain tissue and blood solubility and diffusivity of oxygen and Xe, cerebral blood flow (Q), blood-gas surface tension (σ), atmospheric pressure (P_s), and the partial pressures of carbon dioxide (Pt_{CO_2}) and water vapor (Pt_{H_2O}) in the tissues. We used the following values in the computations: σ = 0.0355 mmHg cm, P_s = 760 mmHg, Pt_{CO_2} = 44 mmHg, Pt_{H_2O} = 47 mmHg, Q = 0.525 cm^3 blood · (cm^3 brain · min)$^{-1}$ at normothermia and mild hyperthermia, and Q = 0.30 cm^3 blood · (cm^3 brain · min)$^{-1}$ for hypothermic conditions.[10]

The model requires input parameters of oxygen and Xe solubility and diffusivity in tissue and blood. Many parameter values for biologic gases are available in the literature, but the list is incomplete for purposes of the analysis considered here. Therefore, one major component of this work was the approximation of missing values for diffusion and solubility coefficients of Xe and oxygen. The parameter estimates, along with literature-derived values, were then used for the simulations of embolism bubbles. Estimates of unknown parameter values were incorporated based on published values of other gases similar to Xe[3,11,12] and were determined as is described in appendixes A and B.

Method of Model Solution

The model incorporating the parameter estimates was solved numerically using the fourth-order Runge-Kutta method in FORTRAN (Lahey Computer Systems, Incline Village, NV) on a Pentium PC. In the case of embolism absorption, time to complete absorption was calculated to within 0.01 min. In the case of bubble growth, doubling time (time required for the bubble to reach twice its initial volume) was calculated to within 0.05 min. All computer simulations were run for bubbles having a 50-nl initial volume entrapped in cerebral vessels. This initial volume is a reasonable size estimate based on *in vivo* studies of bubbles in the microcirculation,[13] and we have previously simulated bubbles this size.[8] Three specific combinations of initial bubble gas composition and delivered gas admixture were simulated: (1) a Xe bubble and oxygen delivery; (2) a Xe bubble and 70% Xe–30% O_2 delivery; and (3) an oxygen bubble and 70% Xe–30% O_2 delivery. Conditions of normothermia, cooling, and

Table 1. Diffusivity Parameter Values

Temperature, °C	Diffusivity, cm^2/s					
	$D_{O_2,water}$	$D_{O_2,blood}$	$D_{O_2,brain}$	$D_{xe,water}$	$D_{xe,blood}$	$D_{xe,brain}$
18	1.96×10^{-5}	1.72×10^{-5}	7.3×10^{-6}	1.01×10^{-5}	8.7×10^{-6}	3.5×10^{-6}
37	3.02×10^{-5}	2.65×10^{-5}	1.12×10^{-5}	1.55×10^{-5}	1.35×10^{-5}	5.4×10^{-6}
39	3.16×10^{-5}	2.77×10^{-5}	1.17×10^{-5}	1.62×10^{-5}	1.41×10^{-5}	5.6×10^{-6}

rewarming during extracorporeal circulation were incorporated by using parameter values (*e.g.*, solubility, diffusivity) for 37°, 18°, and 39°C, respectively. As an additional test, we simulated a 10-μl oxygen bubble introduced into a large, well-mixed, Xe-saturated water reservoir at constant barometric pressure and 37°C. The bubble was allowed to remain spherical. This is an approximation of the experimental conditions studied by Lockwood.[5]

Results

Parameter Estimates

Estimated parameter values for the diffusivity ($D_{O_2,blood}$, $D_{O_2,brain}$, $D_{Xe,blood}$, $D_{Xe,brain}$) and solubility ($L_{O_2,blood}$, $L_{O_2,brain}$, $L_{Xe,blood}$, $L_{Xe,brain}$) of oxygen and Xe in blood and brain are listed in tables 1 and 2, respectively. The estimated values are close to constants determined experimentally for those cases in which the data exist. For example, our estimates of $L_{Xe,blood} = 0.109$ and $L_{Xe,brain} = 0.145$ compare closely with the respective published values of 0.115[3] and 0.153.[12]

Spherical Bubble in Water

The model predicts rapid efflux of oxygen from the bubble accompanied by rapid initial Xe entry. The bubble radial growth rate decays asymptotically to near zero, yielding a Xe bubble having essentially a fixed volume. The volume reaches 99% of its asymptotic limit of 19.78 μl in 7.4 min. Bubble volume is predicted to increase by 50% in the first 1.4 min.

Time History of Bubble Gas Transport Dynamics

Figures 1–5 illustrate our results of the computational predictions of the gas transport dynamics for bubbles of various initial gas compositions and shapes during delivery of various gas mixtures and at various temperatures. In figures 1–4, we demonstrate our findings for behavior of 50-nl bubbles at 37°C. Figure 1, *A* shows results of calculations made for Xe bubbles having initial aspect ratios of 0 (a spherical bubble), 2.6, 10, and 20 (long, slender bubble). Under conditions of oxygen delivery, bubbles are predicted to reabsorb in the range of 15–23 min. The prominent kink present in some curves occurs at the completion of reabsorption of the cylindrical bubble core, with transition to reabsorption of a spherical remnant. Figure 1, *B* shows the time course of the individual gas volumes inside the bubble having $L_o/R_o = 2.6$ shown in figure 1, *A*. Rapid efflux of Xe is predicted to occur in approximately 11 min. Oxygen influx and subsequent reabsorption extends bubble life to approximately 21 min.

In figure 2, *A*, we present the predictions of bubble volume over time for Xe bubbles during delivery of a 70% Xe–30% O_2 mixture. Initial aspect ratios represented are 0, 2.6, 10, and 20. The bubbles seem to shrink initially, but bubble volume then enlarges monotonically. For each of these cases, bubble enlargement occurs by elongation at fixed radius. Figure 2, *B* shows the time course of the individual gases volumes inside the bubble having $L_o/R_o = 2.6$ shown in figure 2, *A*. The Xe volume initially shrinks, with Xe efflux accompanied by oxygen influx. Over time, both Xe and oxygen enter the bubble to promote continued growth.

The case of an embolism bubble having an initial aspect ratio of 0, 2.6, 10, or 20 and first composed entirely of oxygen during 70% Xe–30% O_2 delivery appears in figure 3, *A*. The graph illustrates that unrelenting bubble growth occurs. The volume increase for each case results in an increase in bubble axial dimension while the radius remains constant. Figure 3, *B* shows the time course of the individual gases volumes inside the bubble having $L_o/R_o = 2.6$ shown in figure 3, *A*. The rapid ingress of Xe outstrips the initial elimination of oxygen from the bubble. At longer times, entry of both Xe and

Table 2. Solubility Parameter Values

Temperature, °C	Solubility, $cm^3 \cdot (cm^3\ tissue)^{-1} \cdot atm^{-1}$					
	$L_{O_2,plasma}$	$L_{O_2,blood}$	$L_{O_2,brain}$	$L_{xe,water}$	$L_{xe,blood}$	$L_{xe,brain}$
18	3.0×10^{-6}	3.1×10^{-6}	3.5×10^{-6}	1.28×10^{-5}	1.77×10^{-5}	2.35×10^{-5}
37	2.4×10^{-6}	2.5×10^{-6}	2.8×10^{-6}	7.9×10^{-6}	1.09×10^{-5}	1.45×10^{-5}
39	2.3×10^{-6}	2.4×10^{-6}	2.7×10^{-6}	7.5×10^{-6}	1.04×10^{-5}	1.38×10^{-5}

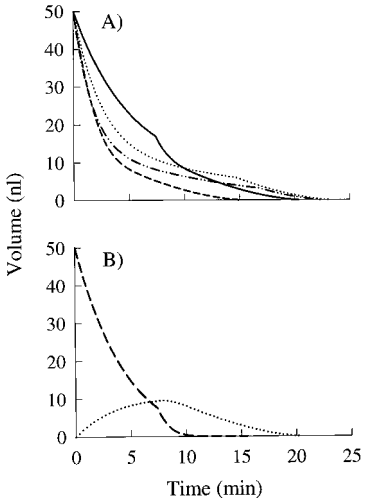

Fig. 1. (*A*) Time course of embolism reabsorption for 50-nl cerebrovascular xenon bubbles during oxygen delivery at 37°C. L_o/R_o = 0 (*dashed line*), 2.6 (*solid line*), 10 (*dotted line*), 20 (*dashed–dotted line*). The kink in the curves occurs at the transition from cylindrical to spherical solutions. (*B*) Individual gas volumes for xenon (*dashed line*) and oxygen (*dotted line*) for L_o/R_o = 2.6.

oxygen into the bubble contributes to its continued growth.

We calculated doubling time, or the time required for a 50-nl bubble to grow to 100 nl. We considered the case in which the bubble is initially comprised of Xe during 70% Xe–30% O_2 delivery. The data are plotted in figure 4 as a function of bubble surface area, rather than aspect ratio, to demonstrate the contribution of surface area to overall gas transport. The single data point represents doubling time for a spherical bubble allowed to grow as a sphere increasing in radius. The curve represents doubling times for bubbles having initial aspect ratios in the range $0 \geq L_o/R_o \geq 25$ but constrained to grow with an

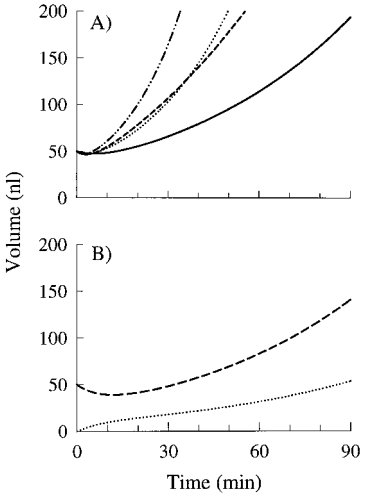

Fig. 2. (*A*) Time course of embolism growth for 50-nl cerebrovascular xenon bubbles during 70% Xe–30% O_2 delivery at 37°C. L_o/R_o = 0 (*dashed line*), 2.6 (*solid line*), 10 (*dotted line*), 20 (*dashed–dotted line*). (*B*) Individual gas volumes for xenon (*dashed line*) and oxygen (*dotted line*) for L_o/R_o = 2.6.

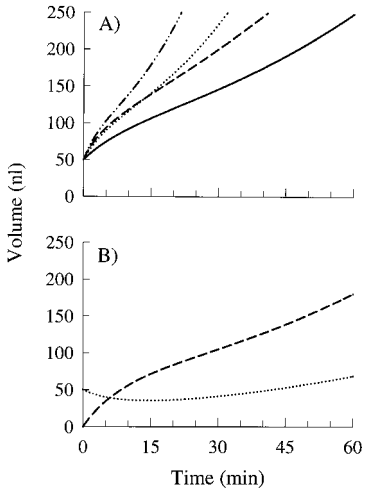

Fig. 3. (*A*) Time course of embolism growth for 50-nl cerebrovascular oxygen bubbles during 70% Xe–30% O_2 delivery at 37°C. L_o/R_o = 0 (*dashed line*), 2.6 (*solid line*), 10 (*dotted line*), 20 (*dashed–dotted line*). (*B*) Individual gas volumes for xenon (*dashed line*) and oxygen (*dotted line*) for L_o/R_o = 2.6.

elongating cylindrical core and with end caps of fixed dimension. For fixed initial volume, the more slender and elongated bubbles enlarge more rapidly. The growth rate is not linearly proportional to bubble surface area.

The effect of temperature on gas transport and bubble size is illustrated in figure 5. For a Xe bubble with L_o/R_o = 10 occurring during oxygen delivery (as in fig. 1, *A*), reabsorption is calculated to be only slightly (~1 min, or < 5%) longer at 39°C than at 18°C, as shown in figure 5, *A*. Predicted bubble growth of a Xe bubble having L_o/R_o = 10 during 70% Xe–30% O_2 delivery appears in figure 5, *B* (corollary to fig. 2, *A*). Bubble volume over time is nearly identical at 37° and 39°C (the two curves overlap) but less at 18°C.

Discussion

Several unanswered questions pertain to the safety of Xe used as a general anesthetic. One major concern is the potential contribution of Xe to gas bubble enlargement in the case of cerebrovascular gas embolism or

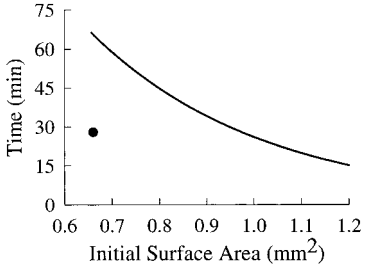

Fig. 4. Predicted time required for a 50-nl xenon cerebrovascular embolism bubble to double its volume at 37°C during 70% Xe–30% O_2 delivery. The single point (*dot*) denotes a spherical bubble growing as a sphere. Elongating bubbles (L_o/R_o > 0) growing at fixed radius appear in the *curve*.

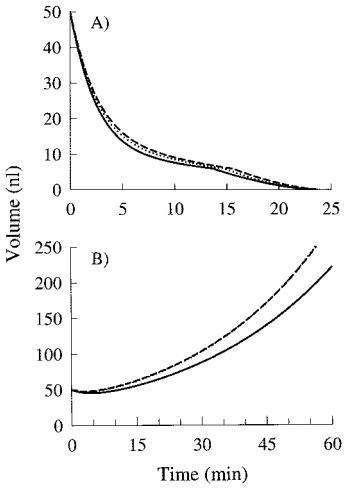

Fig. 5. (*A*) Time course of bubble reabsorption for a 50-nl cerebrovascular xenon bubble with L_o/R_o = 10 during oxygen delivery at 18° (*solid line*), 37° (*dotted line*), or 39°C (*dashed line*). (*B*) Time course of bubble growth for a 50-nl cerebrovascular xenon bubble with L_o/R_o = 10 during 70% Xe–30% O_2 delivery at 18° (*solid line*), 37° (*dotted line*), or 39°C (*dashed line*). Note that curves for 37° and 39°C overlap.

bowel obstruction. Gas embolism is well known to occur in the surgical setting of cardiopulmonary bypass. Cardiopulmonary bypass itself may exacerbate the neurologic injury produced by cerebral arterial air embolism.[14] Delivery of an anesthetic that further promotes bubble growth could prolong ischemic time, increase the size of the vascular territory affected, and thus amplify the injury.

Gas bubbles have been shown to grow in aqueous solution in the presence of Xe,[5] and it is also known that intravascular and extravascular gas bubbles can grow over time in cases of decompression sickness.[8] We used a computational scheme based on a previously validated mathematical model[6,7,9] to predict the behavior of a 50-nl cerebrovascular gas embolism as a function of specific bubble geometry and initial bubble gas composition, given delivery of a particular gas mixture. We chose initial bubble shapes ranging from spherical to long and slender. The particular value L_o/R_o = 2.6 was selected for study because it was associated with prolonged reabsorption of nitrogen-containing bubbles.[6] The model's output does depend on our having used reasonable parameters for the diffusivity and solubility coefficients. Values for coefficients missing from the literature were correlated with and approximated from those constants for gases known and previously published (*e.g.*, tables 1 and 2). The results indicate bubble shrinkage or growth occurs at rates that depend on the initial conditions of bubble shape, exchangeable gas concentration gradients, and temperature.

The three different gas concentration gradient cases used were chosen to illustrate various physical extremes, although the clinical conditions and mechanisms for these extremes to occur may only apply under unusual circumstances. In each of these cases, we consider the tissues already to have been denitrogenated by prolonged oxygen or Xe–oxygen delivery before embolization. We have also neglected the gas transport across the bubble interface that occurs between the moment of bubble introduction into the vasculature and its eventual lodging in the microcirculation, assuming this takes only short time relative to bubble lifetime.[7,9]

An oxygen bubble introduced into a Xe-saturated environment is one case of the largest initial Xe and oxygen gradients across the bubble possible. Although this is not physiologically relevant, we simulated this as a test of our model for comparison of results to those reported for experiment.[5] Our predicted time of 1.4 min for a 50% volume increase was slightly longer than has been measured (~45 s),[5] but the general features of volume increase are recovered considering the variety of differences between the model and the actual conduct of the experiments.

The other, more germane case of the largest possible initial Xe and oxygen gradients across the bubble is a Xe bubble introduced into an oxygen-saturated environment (fig. 1). In this case, the bubble shrinks for all geometries (fig. 1, *A*). As figure 1, *B* shows, the transport strongly favors Xe egress from the bubble to surrounding tissue. The initial oxygen flux into the bubble retards bubble reabsorption to a rate below that of Xe transport. After the bubble's Xe supply has been depleted, the remaining oxygen in the bubble reabsorbs.

The phenomena predicted are quite different with Xe (fig. 2) or oxygen (fig. 3) bubbles lodging in the cerebral vasculature during 70% Xe–30% O_2 delivery. For Xe bubbles, there are initially large Xe and oxygen concentration gradients between the embolism and the cerebral tissue. Although Xe initially passes out of the bubble, oxygen diffuses in, leading to continued dilution of the Xe present in the bubble. Eventually, this reverses the concentration gradient, driving Xe into, rather than out of, the bubble (fig. 2, *B*). Concurrent with Xe diffusion into the bubble, the oxygen gradient is preserved, driving oxygen influx. This mass transport mechanism essentially creates a sink that results in continued bubble growth for all initial bubble aspect ratios (fig. 2, *A*). Growth occurs by axial elongation of the bubble lodged within the vessel, with the bubble filling a greater length of vessel at fixed diameter. This same phenomenon is observed for oxygen bubbles during 70% Xe–30% O_2 delivery, although at different growth rates (fig. 3).

One way to assess the relative rates of bubble growth is to calculate the time required for a bubble to double its volume. The time required for a Xe bubble to double in volume during 70% Xe–30% O_2 delivery is predicted to be greater for bubbles having a more spherical, or slightly elongated aspect ratio (*i.e.*, slightly bigger than a sphere that fills the vessel, fig. 4). The shape with the minimum surface area (*i.e.*, a sphere) enlarges faster if

the radius is allowed to grow than if it is held fixed and the bubble elongates. The difference between these two growth conditions is that the bubble internal pressure remains constant during cylindrical core growth but falls as the bubble radius increases during spherical growth. A drop in internal pressure increases the gradients driving gas into the bubble and speeds growth. Otherwise, for fixed initial bubble volume, a longer and more slender bubble having a larger surface area doubles its volume in less time than if it were nearly spherical. This same effect can be inferred for oxygen bubbles during 70% Xe–30% O_2 delivery from figure 3, *A*. Doubling times are predicted to be in the range of 3–12 min, much faster than the doubling times of comparably shaped Xe bubbles.

The results indicate that both Xe and oxygen bubbles continue to grow during 70% Xe–30% O_2 delivery, whereas Xe bubbles are completely reabsorbed in the absence of a tissue Xe source. The individual parameters such as gas solubility and diffusivity in tissue and blood used to perform these computations are themselves highly temperature dependent, particularly in the range of temperatures typically used for cardiopulmonary bypass (tables 1 and 2). For the data presented in figure 5, *A*, we conducted simulations using values of cerebral blood flow, Q, appropriate for the applicable temperature conditions. We did not find data in the literature for Q at 18°C, so we used Q = 0.30 cm^3 blood · (cm^3 brain · min)$^{-1}$, the value determined by Cook *et al.*[10] for 27°C. We also tested model sensitivity using Q = 0.26 cm^3 blood · (cm^3 brain · min)$^{-1}$, half of the value of Q at 37°C. This analysis demonstrated that reducing Q from 0.525 to 0.26 cm^3 blood · (cm^3 brain · min)$^{-1}$ while keeping the other parameters constant increased the predicted reabsorption time by 1.9% or less. An explanation of this is relatively straightforward. The parameter Q appears in the governing equations and the method of solution adapted from previous work.[6,8] In the model, the value $Q^{1/2}$ is used in the argument of two highly nonlinear functions. Working with an exchange of two gases, we must calculate values of this argument for both Xe and oxygen. Changing Q from 0.525 to 0.3 reduces the argument for Xe and oxygen by 6.1% and 6.5%, respectively, compared to the values at 37°C. Changing Q from 0.525 to 0.26 reduces the arguments for Xe and oxygen by 12.5% and 13.0%, respectively, from their values at 37°C. The solution is relatively insensitive to changes in Q of this order of magnitude.

In fact, as shown in figure 5, the nonlinearity of the overall transport phenomena becomes relatively insensitive to any temperature effect. In the case of bubble reabsorption (fig. 5, *A*), the bubble residence times are within 5% of each other at 18°, 37°, and 39°C. In the case of Xe bubble growth during 70% Xe-30% O_2 delivery, growth rates appear superimposed at 37° and 39°C. Slower growth rates are present under hypothermic conditions, with bubbles taking approximately 15–20% longer to reach the same volume at 18°C compared to 37°C (fig. 5, *B*).

The mass transport in and out of the bubble cannot be easily inferred by inspection of the complex time-dependent nonlinear governing transport equations. There is a thermal competition between solubility effects (a measure of tissue carrying capacity for the gas) and diffusivity effects (a measure of the displacement tendency of gas molecules). Diffusivity increases with increasing temperature, whereas solubility decreases at warmer temperatures. Overall gas exchange depends greatly on the product of the diffusivity and solubility coefficients at each temperature rather than on either one individually. Calculating these products for oxygen and Xe using the data in tables 1 and 2 shows the product for oxygen is 23.6% larger at 18°C than at 37° or 39°C, and the product for Xe is 5.5% smaller at 18°C than at 37° or 39°C. This near constancy of the products, more so for Xe than for oxygen, tracks well with the magnitudes of the predicted behaviors resulting from transport of the two exchangeable gases. In the case of bubble shrinkage, Xe transport dominates the first half of the bubble's existence, and oxygen transport is the dominant mechanism for the second half the bubble's lifetime (fig. 1, *B*). In the case of Xe bubble growth during 70% Xe–30% O_2 delivery, oxygen influx into the bubble (fig. 2, *B*) is the driving force for establishing transport gradients throughout the time period of calculated growth. This accounts for the observed differences in figure 5 over the range of temperatures explored. In general, predictions for a single temperature (say, normothermia) can be directly applied to more extreme temperature conditions encountered if temperature is relatively static. The results cannot be used to infer elements of bubble growth during periods of rapid temperature change, such as active rewarming, because the model does not accommodate events such as tissues becoming supersaturated with a particular gas.

There have not been any *in vivo* studies of gas embolism involving Xe, so it is not clear what the physiologic consequences of bubble growth are after gas embolism lodging during Xe anesthesia. Because bubbles elongate as they grow, the bubble occupies more of the vessel's length over time. This increases the surface area of vascular endothelium in contact with gas, although the cell-damaging effects of this have not been described definitively. Distal bubble elongation should not increase the extent of vascular territory deprived of perfusion because its blood flow will already have been compromised by initial vessel embolization. Bubble growth in the proximal direction could reach to a perfused branch of an arteriolar bifurcation and thus newly deny blood flow into additional tissue. Although Xe has been purported to have neuroprotective qualities,[15,16] there are no data to indicate whether neuroprotection conferred by Xe is sufficient to mitigate the local ischemic injury

that can be induced by cerebral vascular gas embolization. Based on our findings, this could persist for hours with continued bubble growth. Clearly, bubble shrinkage is desired, because bubble reabsorption is likely to be followed by reperfusion.[7,9]

In conclusion, our results show that Xe can promote bubble growth, which could amplify neurologic injury in cerebral arterial gas embolism. Concentration gradients can be manipulated to favor reabsorption of Xe-containing bubbles. Ultimately, ventilation with oxygen at the conclusion of Xe delivery will lead to total bubble reabsorption as Xe is eliminated from the body. The time required for reabsorption will depend on bubble volume and shape as well as the maintenance of perfusion in tissue surrounding the affected area.

References

1. Cullen SC, Gross EG: The anesthetic properties of xenon in animals and human beings, with additional observations on krypton. Science 1951; 113: 580–2
2. Luttropp HH, Romner B, Perhag L, Eskilsson J, Fredriksen S, Werner O: Left ventricular performance and cerebral haemodynamics during xenon anesthesia: A transesophageal echocardiography and transcranial Doppler sonography study. Anaesthesia 1993; 48:1045–9
3. Lynch C III, Baum J, Tenbrinck R: Xenon anesthesia. ANESTHESIOLOGY 2000; 92:865–8
4. Cullen SC, Eger E II, Cullen BF, Gregory P: Observations on the anesthetic effect of the combination of xenon and halothane. ANESTHESIOLOGY 1969; 31:305–9
5. Lockwood G: Expansion of air bubbles in aqueous solutions of nitrous oxide or xenon. Br J Anaesth 2002; 282–6
6. Branger AB, Eckmann DM: Theoretical and experimental intravascular gas embolism absorption dynamics. J Appl Physiol 1999; 87:1287–95
7. Branger AB, Eckmann DM: Accelerated arteriolar gas embolism reabsorption by an exogenous surfactant. ANESTHESIOLOGY 2002; 96:971–9
8. Branger AB, Lambertsen CJ, Eckmann DM: Cerebral gas embolism absorption during hyperbaric therapy: Theory. J Appl Physiol 2001; 90:593–600
9. Eckmann DM, Lomivorotov VN: Microvascular gas embolization clearance following perfluorocarbon administration. J Appl Physiol 2002; 94:860–8
10. Cook DJ, Anderson RE, Michenfelder JD, Oliver WC Jr, Orszulak TA, Daly RC, Bryce RD: Cerebral blood flow during cardiac operations: comparison of Kety-Schmidt and xenon-133 clearance methods. Ann Thoracic Surg 1995; 59: 614–20
11. Vaupel P: Effect of percentual water content in tissues and liquids on the diffusion coefficients of O_2, CO_2, N_2 and H_2. Eur J Physiol 1976; 361:201–4
12. Lango T, Morland T, Brubakk AO: Diffusion coefficients and solubility coefficients for gases in biological fluids and tissues: A review. Undersea Hyperbaric Med 1996; 24:247–72
13. McDermott JJ, Dutka AJ, Koller WA, Flynn ET: Effects of an increased PO_2 during recompression therapy for the treatment of experimental cerebral arterial gas embolism. Undersea Biomed Res 1992; 19:403–13
14. Hindman BJ, Dexter F, Enomoto S, Subieta A, Smith T, Cutkomp J: Recovery of evoked potential amplitude after cerebral arterial air embolism in the rabbit. ANESTHESIOLOGY 1998; 88:696–707
15. Ma D, Wilhelm S, Maze M, Franks NP: Neuroprotective and neurotoxic properties of the 'inert' gas, xenon. Br J Anaesth 2002; 89:739–46
16. Ma D, Yang H, Lynch J, Franks NP, Maze M, Grocott HP: Xenon attenuates cardiopulmonary bypass-induced neurologic and neurocognitive dysfunction in the rat. ANESTHESIOLOGY 2003; 98:690–8
17. Lentner C: Geigy Scientific Tables. Vol 1. West Caldwell, New Jersey, Ciba-Geigy, 1981, pp 223
18. Evans AL, Busuttil A, Gillespie FC, Unsworth J: The rate of clearance of xenon from rat liver sections in vitro and its significance in relation to intracellular diffusion rates. Physics Med Biol 1974; 19:303–16
19. Bird RB, Stewart WE, Lightfoot EN: Transport Phenomena. New York, John Wiley & Sons, 1976, pp 505
20. Meyer M, Tebbe U, Piiper J: Solubility of inert gases in dog blood and skeletal muscle. Eur J Physiol 1980; 384:131–4
21. Hlastala MP, Meyer M, Riepl G, Scheid P: Solubility of helium, argon, and sulfur hexafluoride in human blood measured by mass spectrometry. Undersea Biomed Res 1980; 7:297–304
22. Levitt MD, Levitt DG: Use of inert gases to study the interaction of blood flow and diffusion during passive absorption from the gastrointestinal tract of the rat. J Clin Invest 1973; 52:1852–62
23. Carles AC, Kawashiro T, Piiper J: Solubility of various inert gases in rat skeletal muscle. Eur J Physiol 1975; 359:209–18
24. Mapleson WW, Evans DE, Flook V: The variability of partition coefficients for nitrous oxide and cyclopropane in the rabbit. Br J Anaesth 1970; 42:1033–41
25. Christoforides C, Laasberg LH, Hedley-Whyte J: Effect of temperature on solubility of O_2 in human plasma. J Appl Physiol 1969; 26:56–60
26. Siesjø B: The solubility of CO_2 in cerebral cortical tissue of cats. Acta Physiol Scand 1962; 55:325–41
27. Van Slyke DD, Dillon RT, Margaria R: Studies of gas and electrolyte equilibria in blood: XVIII. Solubility and physical state of atmospheric nitrogen in blood cells and plasma. J Biol Chem 1934; 105:541–96
28. Campbell JA, Hill L: Concerning the amount of nitrogen gas in the tissues and its removal by breathing almost pure oxygen. J Physiol (Lond) 1931; 71: 309–22

Appendix A

Determination of Diffusion Coefficients Based on Tissue Water Content

Estimates of the diffusion coefficient values not available in the literature were based on known values and their relation to the fractional water content, w, of brain tissue and blood.[11] The diffusion coefficient of a particular gas i in a tissue with fractional water content w, $D_{i,\text{tissue}}(w)$, is given by[17]:

$$D_{i,\text{tissue}}(w) = D_{i,\text{water}} \cdot e^{-v(-w+1)} \quad (1)$$

in which $D_{i,\text{ water}}$ is the diffusivity of gas species i in water and the coefficient v is derived from experiments. Equation 1 holds for $0.65 \geq w \geq 1$.[11] Values of v at 37°C are known for oxygen (4.4), carbon dioxide (3.9), nitrogen (4.3), and hydrogen (4.6).[11] A value of v for xenon must be estimated because a value from experiments has not been published.

First, values for w in skin, liver, skeletal muscle, brain, lung, spleen, heart, and kidney range from 0.69 to 0.82,[17] with w approximately 0.77 in the adult human brain and w approximately 0.96 in blood. For rat liver, w is approximately 0.7.[17] Known diffusivities at 37°C include $D_{\text{Xe,rat liver}} = 0.38 \times 10^{-5}$ cm^2/s,[18] $D_{\text{Xe,water}} = 1.55 \times 10^{-5}$ cm^2/s,[18] and $D_{O_2,\text{water}} = 3.02 \times 10^{-5}$ cm^2/s.[19] From equation 1, a value $v = 4.7$ is estimated for xenon in tissue. It follows that $D_{O_2,\text{brain}} = 1.11 \times 10^{-5}$ cm^2/s and $D_{\text{Xe,brain}} = 0.54 \times 10^{-5}$ cm^2/s at 37°C.

Temperature Dependence of Diffusion Coefficients

Lango *et al.*[12] showed an expression that accurately reflects the temperature dependence of diffusion coefficients is:

$$D = ae^{bT} \quad (2)$$

in which T is the temperature (°C), and the constants a and b are experimentally determined. Values of a and b have been published for many gases, including oxygen ($a = 1.40$, $b = 0.023$), but not for xenon.[12] Other published values of b range from 0.019 (nitrous oxide) to 0.027 (argon). Values do not correlate in any discernible fashion with molecular weight, molecular size, or other molecular features. We chose $b = 0.023$ for xenon because this was the mean of seven published values[12] and it falls in the middle of their range. Table 1 lists the values of the diffusion coefficients known and estimated using equations 1 and 2 and the relevant constants denoted above.

Appendix B

Determination of Solubility Coefficients

The solubility of oxygen in human plasma, $L_{O2,\text{plasma}}$, at 37°C is well documented[12] and is within 5% of $L_{O_2,\text{blood}}$, the solubility of oxygen in whole blood. We calculated $L_{O_2,\text{blood}} = L_{O_2,\text{plasma}}/0.96$ using the published data of oxygen solubility in plasma at the three temperatures of interest. Numerous values of the solubility of various gases in tissues and blood appear in the literature.[20–28] The ratio $L_{i,\text{brain}}/L_{i,\text{blood}}$ for different gases (denoted by i) consistently falls in the range of approx-

imately 1.07–1.15. For rabbits, $L_{O_2,brain}/L_{O_2,blood} = 1.11$.[12,24] We calculated $L_{O_2,brain} = 1.11\ L_{O_2,blood} = 1.156\ L_{O_2,plasma}$ using known values of $L_{O_2,plasma}$ for 18°, 37°, and 39°C.

We plotted known Ostwald solubility coefficients for xenon in water, $L_{Xe,water}$, against temperature, T, at 0, 20, 30, and 37°C.[3,19] We fitted the data to a first-order exponential equation,

$$L_{Xe,water} = 0.2016e^{-0.0254 3T} \quad (3)$$

resulting in a least-squares correlation coefficient $r = 0.997$. We then calculated values of $L_{Xe,water}$ with equation 3. The same approach used to approximate $L_{O_2,brain}$ and $L_{O_2,blood}$ was used to estimate $L_{Xe,blood}$. We correlated solubilities of the gas species in different media at the same temperature.[20–28] The relation between known values of $L_{Xe,water}$,[3,19] $L_{Xe,blood}$,[3] and $L_{Xe,brain}$[12] at 37°C is approximated by: $L_{Xe,blood} = 1.385\ L_{Xe,water}$; and $L_{Xe,brain} = 1.33\ L_{Xe,blood}$. Estimated values of $L_{Xe,blood}$ and $L_{Xe,brain}$ were then calculated using values of $L_{Xe,water}$ determined from equation 3. All the estimated solubility parameter values are listed in table 2.